PCCP

Elucidation of the atomic-scale processes of dissociative adsorption and spillover of hydrogen on the single atom alloy catalyst Pd/Cu(111)

Journal:	*Physical Chemistry Chemical Physics*
Manuscript ID	CP-ART-04-2022-001652.R2
Article Type:	Paper
Date Submitted by the Author:	09-Aug-2022
Complete List of Authors:	Osada, Wataru; The University of Tokyo, The Institute for Solid State Physics Tanaka, Shunsuke; The University of Tokyo, The Institute for Solid State Physics Mukai, Kozo; The University of Tokyo, The Institute for Solid State Physics Kawamura, Mitsuaki; The University of Tokyo, The Institute for Solid State Physics Choi, YoungHyun; The University of Tokyo, The Institute for Solid State Physics Ozaki, Fumihiko; The University of Tokyo, The Institute for Solid State Physics Ozaki, Taisuke; The University of Tokyo, The Institute for Solid State Physics Yoshinobu, J.; The University of Tokyo, The Institute for Solid State Physics

ARTICLE

Elucidation of the atomic-scale processes of dissociative adsorption and spillover of hydrogen on the single atom alloy catalyst Pd/Cu(111)

Wataru Osada, [a] Shunsuke Tanaka, [a] Kozo Mukai, [a] Mitsuaki Kawamura, [a] YoungHyun Choi, [a] Fumihiko Ozaki, [a] Taisuke Ozaki, [a] and Jun Yoshinobu *[a]

Hydrogen spillover is a crucial process in the selective hydrogenation reactions on Pd/Cu single atom alloy catalysts. In this study, we report the atomic-scale perspective of these processes on the single atom alloy catalyst Pd/Cu (111) based on the experimental and theoretical results, including infrared reflection absorption spectroscopy (IRAS), temperature programmed desorption (TPD), high-resolution X-ray photoelectron spectroscopy (HR-XPS), and density functional theory (DFT) calculations for core-level excitation. The hydrogen spillover onto Cu(111) was successfully observed in real-time using time-resolved IRAS measurements at 80 K. The chemical shifts of Pd $3d_{5/2}$ indicate that H_2 is dissociated and adsorbed at the Pd site. In addition, the "two-step" chemical shift of the Pd $3d_{5/2}$ binding energy was observed, indicating two types of hydrogen adsorption states at the Pd site. The proposed mechanism of the hydrogen dissociation and spillover processes includes (i) a hydrogen molecule is dissociated at a Pd site, and the hydrogen atoms are adsorbed on the Pd site, (ii) the number of hydrogen atoms on the Pd site increases up to three, and (iii) the hydrogen atoms will spill over onto the Cu surface.

Introduction

The utilization of hydrogen in industry indicates its significant importance for our modern society because many indispensable processes consist of chemical reactions involving hydrogen: synthesis of chemical feedstocks such as methanol and ammonia, petroleum refining, energy source through fuel cell systems, and so forth.[1–3] In these reactions, atomic hydrogen, proton, or hydride play an important role because of their high reactivity.[4] Therefore, dissociation of molecular hydrogen is an essential elementary step in hydrogenation reactions, where the active sites for hydrogen dissociation are necessary. Transition metals such as Ni, Pt, and Pd have been widely used for various hydrogenation reactions because of their high activity for hydrogen dissociation.[2,5,6] In practice, a second or more metals are usually added to these metal catalysts as the promoters, which improve the catalytic activity, selectivity, and stability.[6] For example, in the acetylene hydrogenation on the Pd catalyst, the selectivity to ethylene is improved by adding Ag.[7] Thus, alloying enhances catalytic properties.[8,9]

In recent years, single atom alloy catalysts (SAACs) have been attracting much attention due to their excellent properties, such as high activity and selectivity[10–13] and

resistance to deactivation via coke formation or CO poisoning.[10–13] In the SAACs, active metal atoms are highly diluted and atomically dispersed on an inert but selective metal surface. Kyriakou *et al.* first reported the catalytic reaction using SAAC;[14] acetylene/styrene was hydrogenated to ethylene/ethylbenzene on Pd/Cu(111) with more than 95% selectivity. Thereafter, many researchers have investigated many catalytic reactions on various SAACs, such as Pd/Cu,[13–20] Pd/Au,[21] Pt/Cu,[12,16,17,22–24] Ni/Cu,[17] and so forth.[10] The proposed hydrogenation mechanism in these studies is as follows:[12,14,20] (i) the molecular hydrogen is dissociated at the active metal atom site, such as Pd, (ii) the hydrogen atoms spill over onto the inert host surface (for example, Cu), (iii) the spilled hydrogen atoms react with other molecules (e.g. acetylene), and (iv) product molecules (e.g. ethylene) are immediately desorbed due to the weak interaction with the host metal surface. Thus, the hydrogenation on the host surface is a key factor of the high selectivity. Therefore, hydrogen spillover onto the host metal surfaces is a crucial process for selective hydrogenation.

Based on such background, the hydrogen dissociation and spillover processes on the Pd/Cu SAAC surfaces have been investigated by both experimental and theoretical researchers.[14,15,20,25–31] The spilled hydrogen atoms on the host Cu surfaces were visualized using scanning tunneling microscopy (STM).[14,15,25] In addition, Kyriakou *et al.* reported the adsorption of many more hydrogen atoms on the surface than deposited Pd atoms based on the thermal desorption spectra.[14] These results indicated that hydrogen atoms are adsorbed on the Cu host sites on the Pd/Cu SAAC surface.

a. The Institute for Solid State Physics, The University of Tokyo, 5-1-5 Kashiwanoha, Kashiwa, Chiba 277-8581, Japan

However, the dissociative adsorption at the Pd site and subsequent spillover processes of hydrogen have not been continuously observed experimentally. Although theoretical studies have supported that the Pd single atom site can act as an active site for hydrogen dissociation,[26,29–31] there is little experimental evidence for the initial dissociative adsorption of H_2 and the spillover process so far.

In this paper, we conducted experiments including infrared reflection absorption spectroscopy (IRAS), temperature programmed desorption (TPD), and high-resolution X-ray photoelectron spectroscopy (HR-XPS), as well as density functional theory (DFT) calculations, to investigate the dissociative adsorption of the hydrogen and spillover process on the prepared Pd/Cu(111) surface at ~80 K. The present experiments directly observed the initial dissociative adsorption of hydrogen at Pd sites and the subsequent spillover process onto the Cu sites. Based on the present experimental and theoretical results, we discuss the hydrogen dissociation and spillover processes on the Pd/Cu(111) and propose an atomic-scale perspective of these processes on the Pd/Cu SAAC surface.

Experimental and Theoretical Methods

IRAS and TPD experiments were conducted in the UHV chamber equipped with a Pd evaporator. The base pressure was lower than 4×10^{-8} Pa. The sample was cooled at 83 K by liquid nitrogen. IRAS measurements were performed using a Fourier transform infrared spectrometer (Bruker, IFS/66v) and a mercury-cadmium-telluride (MCT) detector. We performed time-resolved IRAS measurements during H_2 exposure, where the pressure was maintained at 4.0×10^{-4} Pa by using a cold-cathode gauge. All IRAS spectra were obtained with 4 cm^{-1} resolution and 500 scans. The reference spectrum was measured on the clean Pd/Cu(111) surface just before the H_2 exposure. The coverage of the adsorbed hydrogen atoms (ϑ_H) was estimated from the H-Cu vibrational peak area. Mudiyanselage *et al.* reported that the integrated absorbance of the H-Cu peak at 1150 cm^{-1} linearly changed with the ϑ_H.[32] The vibrational peak area was converted to the coverage, which was calibrated from the desorption peak area obtained from TPD performed just after the IRAS measurements. The estimation of ϑ_H from TPD results was based on the comparing the desorption peak area with that on the surface exposed to 10000 L of H_2, where we assumed that the Pd/Cu(111) surface was almost saturated by H atoms. The saturation coverage of H atoms on Pd/Cu(111) is assumed to be 0.67 ML, which is equivalent to that on Cu(111).[33] TPD measurements were performed using a quadrupole mass spectrometer (Balzers, Prisma QMS 200). The sample was heated at a rate of 1.1 K s^{-1}. A thoriated tungsten filament was used to heat the sample. The sample temperature was measured with a K-type thermocouple.

High-resolution XPS measurements were performed in another UHV chamber equipped with a hemispherical electron energy analyzer (SPECS, Phoibos 100) and a quadrupole mass spectrometer (Balzers, Prisma QMS 200) at BL-13B of the synchrotron light source (Photon Factory, KEK, Japan). The base

pressure was ~5×10^{-10} Torr. The prepared Pd/Cu(111) surface was exposed to H_2 at ~80 K up to 800 L. The Cu 3p, Pd 3d$_{5/2}$, C 1s, and O 1s XPS spectra were measured using a photon energy of 680 eV. The zero binding energy was taken at the Fermi energy of the Cu substrate. All XPS measurements were conducted with a normal emission condition. The incident angle of the X-ray was 45 degrees from the surface normal.

The clean Cu (111) surface was prepared by several cycles of Ne$^+$ sputtering and annealing at 673 K for 2 min. In IRAS and TPD, the cleanness of the Cu(111) surface was confirmed by IRAS and TPD spectra of the CO adsorbed surface.[34,35] In HR-XPS, we confirmed the clean Cu(111) surface by the observation of (1 × 1) LEED pattern and XPS measurement. Pd atoms were deposited on the clean Cu(111) surface by resistive heating of a Pd wire wrapped on a W filament. The diameters of the Pd and W wires were 0.1 mm and 0.2 mm, respectively. During the deposition, the temperature of Cu samples was maintained at 380 K, where the deposited Pd atoms were atomically dispersed and alloyed on the Cu surface.[36]

Gaseous H_2 was introduced into the UHV chamber through a variable leak valve in both XPS and IRAS/TPD experiments.

The coverage of the deposited Pd (ϑ_{Pd}) was estimated from H_2-TPD in IRAS and TPD experiments. Kyriakou *et al.* reported the symmetric desorption spectra for the recombination of the adsorbed H atoms at 210 K on 0.01 ML Pd/Cu(111).[14] In the low ϑ_{Pd} region, the desorption temperature of H_2 changed as a function of ϑ_{Pd}.[11,17] In HR-XPS, we estimated ϑ_{Pd} based on the peak area ratio of Pd 3d$_{5/2}$/Cu 3p$_{3/2}$. The observed peak areas were calibrated by photoionization cross sections considering asymmetry parameters.[37,38] In addition, the total area of the Cu 3p peak was multiplied by 2/3 to obtain the intensity of Cu 3p$_{3/2}$. Finally, we applied the depth distribution function with the straight-line approximation, where the escape probability of photoelectrons is assumed to decay exponentially with the depth of their generated points,[39] to evaluate the contribution of the surface component in the observed Cu 3p signal.

DFT calculations were performed using OpenMX code.[40,41] For the exchange-correlation functional, the generalized gradient approximation with the Perdew-Burke-Ernzerhof functional (GGA-PBE) was used.[42] The Pd/Cu(111) surface was modeled by a four atomic-layer slab with a (4 × 4) unit cell separated by a vacuum of ~15 Å thickness. Cu atoms in the bottom two layers were fixed in their bulk position, which was determined by the experimental lattice constant of copper. Cu and Pd atoms in the top two layers were allowed to relax with hydrogen atoms. In geometrical optimization, conventional pseudopotentials and optimized basis functions provided on the OpenMX website were used.[43–47] The adsorption energy per one hydrogen atom, ΔH_{ad} was calculated with the following formula:

$$\Delta H_{ad} = \left\{ E_{\text{H-adsorbed}} - \left(E_{\text{clean}} + E_{H_2,\text{gas}} \times \frac{n}{2} \right) \right\} / n$$

where, E and n are the total energy and the number of adsorbed hydrogen atoms, respectively. The van der Waals (vdW) interaction was taken into account by the density functional dispersion correction approach (DFT-D3).[48,49] In calculations for core-level excitation, the fully relativistic pseudopotential and

pseudo-atomic orbitals of Pd for core level excitation were used.[50,51] The fixed empty atoms with pseudo-atomic orbitals for hydrogen were placed on all vacant hollow sites in all calculations.

Results and discussion

IRAS: real-time observation of the spillover process

We conducted time-resolved IRAS measurements to detect surface vibrational spectra as a function of time during the exposure to gaseous H_2. Figure 1 (a) shows a series of time-resolved IRAS spectra in the region of 900-1300 cm^{-1}. The indicated times are the elapsed time from the start of H_2 exposure, t. The H_2 pressure was 4 ×10^{-4} Pa, and the exposure was stopped at t = 1200 s. Therefore, the total H_2 exposure was 3600 L. In the present measurements, we estimated the Pd coverage to be ~ 0.01 ML from the TPD results, where the symmetric desorption peaks were observed at 220 K. The interpretation of TPD results will be discussed later. The vibrational peaks were observed at 1143-1135 cm^{-1}. In the previous studies, Cu(111) surfaces were exposed to atomic hydrogen, and the H-Cu vibrational peaks were observed at 1151-1137 cm^{-1}.[32,52] Therefore, we assign the vibrational peaks in Fig. 1 (a) to the H-Cu vibrational mode.

We conducted the TPD measurement after the present IRAS, and estimated the hydrogen coverage (ϑ_H) to be 0.23 ML. The H-Cu peak areas were converted to the ϑ_H, assuming that the peak area is in proportion to the coverage.[32] Figure 1 (b) shows the change of the H-Cu peak area (ϑ_H, right-hand axis) as a function of elapsed time. The amount of hydrogen atoms

adsorbed on the Cu surface clearly increased with the H_2 exposure, indicating that adsorbed hydrogen atoms migrated from the Pd sites onto the Cu surface. In other words, the present IRAS measurements observed the hydrogen spillover in real-time. The line fitting in Fig. 1 (b) indicates that the hydrogen spillover started at 263 s delay from the start of H_2 exposure (t=0). This can be related to the rate of the spillover process, which will be discussed below.

The slope of the dashed line in Fig. 1 (b) gives the spillover rate of 1.4±0.1 × 10^{-4} ML s^{-1}. This slow rate of spillover indicates that the dissociated hydrogen atoms could remain on the Pd site for some time at ~80 K. Therefore, the adsorption of hydrogen atoms on the Cu sites needs a relatively long time for IRAS measurements. Thus, we can conclude that the ~270 s delay of the spillover starting from the start of the H_2 exposure originated from the slowness of the spillover process. In addition, the peak area increased even after the H_2 dosing was stopped; ~0.1 ML of the hydrogen atoms additionally spilled over onto the Cu sites. Because the Pd coverage (~0.01 ML) was considerably low compared with this increased hydrogen, the source supplying hydrogen to the surface should exist even after the stop of H_2 dosing. The residual hydrogen in the background is a possible origin.

The frequency of the H-Cu vibrational peak has shifted to lower wavenumber as a function of the exposure. This redshift was probably due to the increase in ϑ_H. In addition, a small amount of adsorbed CO from background could induce the redshift; Mudiyanselage *et al.* reported that not only the increase in ϑ_H but also the co-adsorption of CO caused the redshift of the H-Cu vibrational frequency on Cu(111).[32] Our IRAS spectra detected a vibrational peak at 2073 cm^{-1} (see the inset of Fig. 1 (a)), which can be assigned to the CO adsorbed on the Cu surface.[35] The vibrational peaks of CO adsorbed on the Pd atom embedded in Cu(111) were observed at 2065-2068 cm^{-1}.[53] Note that CO molecules could be adsorbed on not only the Cu site but also the Pd site because the Pd site is more stable adsorption site.[15] The absence of the vibrational peak for the CO on the Pd site was probably due to the dipole-dipole coupling, i.e., the intensity for the lower frequency vibrational mode (CO-Pd) was stolen by the higher frequency mode (CO-Cu).[54] We estimate the CO coverage after IRAS to be 0.04 ML based on the vibrational peak intensity.

TPD: recombinative desorption of hydrogen atoms

Figure 2 shows the TPD results measured on the prepared Pd/Cu(111) surface as a function of the H_2 exposure. The desorption peaks of hydrogen molecules were observed at 220 K. The present desorption spectra were similar to that on 0.01 ML Pd/Cu(111) reported by the previous studies.[14,20] The symmetric shapes of these peaks indicate the second-order kinetics, i.e., the recombinative desorption of adsorbed hydrogen atoms. In Fig. 2, temperatures at desorption maxima, T_p, were almost constant as a function of H_2 exposure. This tendency is consistent with a previous result reported by Kyriakou *et al.*[14] In the case of the second-order desorption, T_p should shift to lower temperatures with increasing the initial
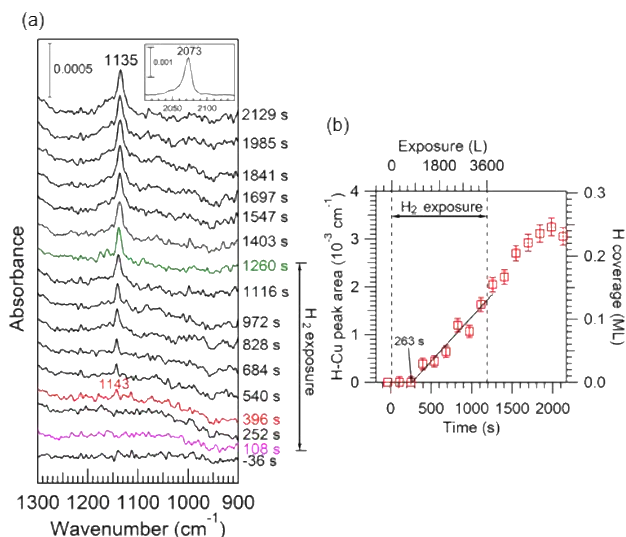
Fig. 1 (a) Time-resolved IRAS spectra during H_2 exposure onto the Pd/Cu(111) surface (ϑ_{Pd} = ~0.01 ML). The indicated time, t, is the elapsed time from the start of H_2 dosing. The vibrational peak first appeared at t = 396 s (red spectrum). The pressure was maintained at 4.0 × 10^{-4} Pa during the H_2 exposure. The inset shows the spectrum at 2129 s in the CO region; the CO coverage is ~0.04 ML. The measurement time for each spectrum was ~143 s. The labelled times mean the end times of each measurement. (b) The change of the hydrogen coverage as a function of elapsed time. The H coverage was estimated from the H-Cu peak area, where the H-Cu peak areas were converted to the coverage based on the TPD results. The error bars are for the left axis. The sample was cooled to ~80 K by liquid nitrogen before H_2 exposure.
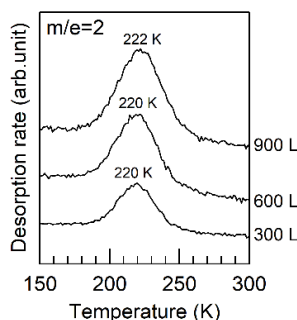
Fig. 2 TPD results measured on the Pd/Cu(111) surface (θ_{Pd} = ~0.01 ML) as a function of the H_2 exposure. The peak areas of 300, 600, and 900 L spectra correspond to the coverages of 0.16, 0.30, and 0.41 ML, respectively.

coverage if the activation energy for desorption, E_d, is constant. The constant peak temperatures in Fig. 2 indicate that the E_d increased with increasing the hydrogen coverage which suggests that the dissociation barrier of gaseous H_2 could be increased. We consider that the single Pd sites on Cu(111) may become less reactive by H adsorption, which raises the activation energy for the dissociative adsorption of H_2.

We estimated ϑ_H to be 0.41 ML for the 900 L exposure, which seems to be inconsistent with the above IRAS results. This discrepancy was probably due to the position (orientation) of the sample surface with respect to the aperture of a gas introduction tube from a variable leak valve. While the sample surface had its back to the aperture in IRAS measurements, it saw the aperture in TPD experiments. Thus, the collision rate of H_2 molecules onto the surface was different between IRAS and TPD.

HR-XPS: dissociative adsorption of H_2 at the Pd sites

We performed HR-XPS measurements to investigate the effect of hydrogen adsorption on the Pd atoms of the Pd/Cu(111) surface at 80 K. The results on Pd $3d_{5/2}$ are shown in Fig. 3 (a) as a function of the experimental processes. Here, we estimate ϑ_{Pd} as follows. The observed peak area ratio of Pd $3d_{5/2}$/ Cu 3p was 0.064 on the Pd deposited surface (the spectrum A in Fig. 3 (a)). The photoionization cross section of Pd $3d_{5/2}$ is 7.4 times larger than that of Cu $3p_{3/2}$ considering the asymmetry parameters.[38] The photoelectrons from the outermost Cu atoms in the total Cu 3p intensity were evaluated to be 20%, where the thickness of the Cu layer and inelastic mean free path were assumed to be 2.56 and 11.39 Å, respectively. The former is the separation between (111) planes based on the lattice constant, and the latter is calculated by the "NIST ELECTRON EFFECTIVE-ATTENUATION-LENGTH DATABASE".[55] Finally, the total peak area of Cu 3p was calibrated by the factor of 2/3. Therefore, we estimate that ϑ_{Pd} on the prepared Pd/Cu(111) surface was 0.06 ML, where we safely assume that the deposited Pd atoms are atomically dispersed.[20,53]

In the spectrum A in Fig. 3 (a), which was measured on the as-deposited surface at room temperature, a single peak was observed at 335.3 eV. The single component of the observed Pd $3d_{5/2}$ peak and the small ϑ_{Pd} support that the prepared Pd/Cu(111) surface is a single atom alloy surface. After cooling to 80 K, a very small component appeared at 335.7 eV, and the

intensity of this peak increased with H_2 exposure. The peak at 336.4 eV developed with the further increase of H_2 exposure. Thus, three components were observed in a series of the present XPS spectra. The change in the integrated intensity for each component was summarized in Fig. 3 (b), where the intensity is normalized by the total peak area of each spectrum.

The blue component, 335.3 eV, which decreased with H_2 exposure and disappeared at 800 L, can be attributed to the Pd atoms lying on the clean surface. The binding energy of 335.3 eV is different from that on both the pure Pd(111) surface (334.6-334.7 eV)[56,57] and the Pd-Cu alloy surface (335.82 eV).[58] Thus, the Pd atom embedded in the Cu(111) surface has a characteristic electronic state, which can be confirmed by the present theoretical calculation (discussed later). The binding energy of the green component (335.7 eV) is higher by 0.4 eV than that of the blue. This binding energy shift is similar to the hydrogen-induced shift for the Pd-Cu alloy, 0.35 eV.[58] Therefore, we can assign the Pd $3d_{5/2}$ peak at 335.7 eV to the hydrogen-adsorbed Pd atoms (Pd-H). The increase in the intensity of the green component with H_2 exposure up to 50 L also supports this assignment. While the green peak decreased at 800 L H_2, the magenta peak at 336.4 eV monotonically increased with H_2 exposure. The binding energy shift between the blue and magenta components was 1.1 eV. Such a large shift has not been reported on the hydrogen adsorbed/absorbed Pd or Pd-based alloy to the best of our knowledge. In the case of the Pd hydride, the chemical shift of 0.34-0.36 eV was reported.[59] Note that, there was little change in the Pd $3d_{5/2}$ spectrum with the heating to 150 K, where H_2O and CO were almost desorbed from the Cu surface (the spectrum F in Fig. 3 (a)).[34,60] Therefore, we can exclude H_2O and CO as the origin of the magenta component, and we conclude that the peak at 336.4 eV was induced by hydrogen adsorption on the Pd/Cu(111) surface.
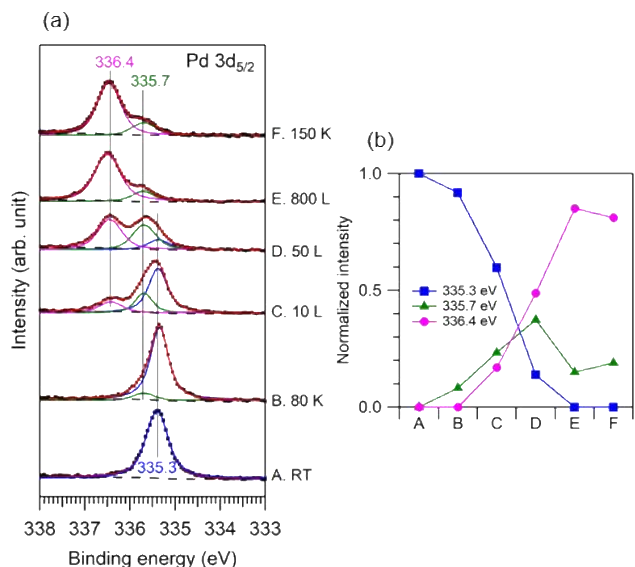
Fig. 3 HR-XPS results measured on the Pd/Cu(111) surface (ϑ_{Pd} = 0.06 ML). (a) The Pd3d$_{5/2}$ spectra were taken on the clean Pd/Cu(111) surface at room temperature (A), 80 K (B), and after H$_2$ exposure of 10 L (C), 50 L (D), 800 L (E), and at 150 K (F). These spectra are fitted by Voigt peaks with a Shirley-background. (b) The change in the normalized intensity of each component as a function of the experimental process.

As discussed above, we assign the observed Pd 3d$_{5/2}$ peaks at 335.7 and 336.4 eV to the hydrogen-adsorbed Pd atom. As shown in Fig. 3 (b), after 800 L exposure, the intensity of the 335.7 eV peak decreased, but the 336.4 eV increased. This behaviour is interpreted to indicate that the binding energy of the Pd atoms observed as the component at 335.7 eV further shifted to higher with increasing H$_2$ exposure. We consider that the observed binding energy may reflect the number of the adsorbed hydrogen atoms around the Pd site; the peaks at 335.7 and 336.4 eV were attributed to the Pd atoms with the low and high hydrogen coverage, respectively. This "two-step" binding energy shift will be further investigated by DFT calculations in the following section.

DFT calculations

The adsorption structure The above experimental results indicate that there are at least two types of the hydrogen adsorbed Pd state on the Pd/Cu(111) surface. To confirm this hypothesis, we systematically performed DFT calculations to explore the stable structures of the hydrogen adsorbed Pd/Cu SAAC surface. In the present calculations, we exclude the configurations where two or more Pd atoms are adjacent. Some previous studies reported the Pd atoms embedded in the Cu(111) surface prefer to be isolated from each other,[36,61,62] and the present Pd coverages correspond to 0.06 ML.

Figure 4 shows the model structures of the clean and hydrogen adsorbed Pd/Cu(111) surfaces with various numbers and configurations of H atoms. We performed calculations to optimize the geometry for each structure and obtained the adsorption energy per one hydrogen atom, ΔH_{ad} (Table 1). The most stable adsorption site for one hydrogen atom is an hcp-hollow site consisting of one Pd atom and two Cu atoms (Fig. 4 (b), "Pd-hcp site"); ΔH_{ad} = −0.261 eV. That on the Pd-fcc site was

Table 1. The calculated adsorption energies per one hydrogen atom, ΔH_{ad}, on various H-adsorbed Pd/Cu(111) surfaces. The labels and configurations in the first and second column correspond to those in Fig. 3. ΔH_{ad} was calculated with the following formula: $\{E_{H\text{-}ad} - (E_{clean} + E_{H2,\,gas*n/2})\}/n$, n is the number of the adsorbed H atoms.

Label	Configuration	ΔH_{ad} (eV)
(a)	Clean	0
(b)	1H-hcp	−0.261
(c)	2H-2NN	−0.262
(d)	2H-3NN	−0.248
(e)	2H-Pd&Cu	−0.192
(f)	3H-hcp	−0.253
(g)	3H-Pd&Cu	−0.225
(h)	4H-all hollow	−0.115
(i)	4H-hcp&top	−0.062
(j)	4H-near	−0.220
(k)	4H-middle	−0.237
(l)	4H-far	−0.245

-0.239 eV (not shown in Fig. 4 and Table 1), slightly less stable than Fig. 4 (b). This tendency is consistent with the previous study.[26]

In the case of two adsorbed hydrogen atoms, the second nearest neighbor occupation of the Pd-hcp site is the most stable (Fig. 4 (c)). Although the previous studies have assumed
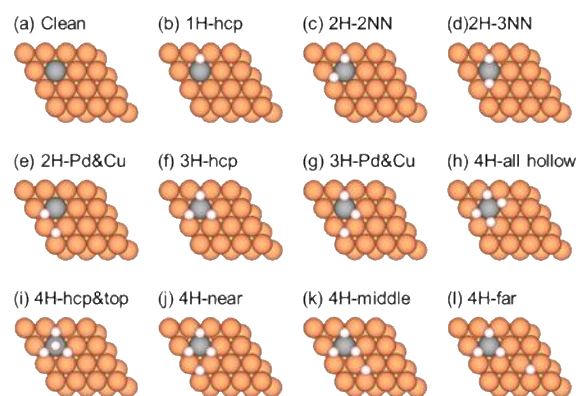
Fig. 4 Structural models of the (a) clean and (b)-(l) hydrogen adsorbed Pd/Cu(111) surface used in DFT calculations. Empty atoms with pseudo-atomic orbitals for hydrogen were placed on all vacant hollow sites for each structure (not shown here). The orange, gray, and small white spheres present the Cu, Pd, and H atoms, respectively.

the structure with the hydrogen atoms on the third nearest neighbor of the hollow site (Fig. 4 (d)) as the adsorption structure after H$_2$ was dissociated on the Pd site,[11,27,29] the structure in Fig. 4 (d) is slightly less stable than that in Fig. 4 (c). Therefore, the adsorption structure in Fig. 4 (d) is not the most stable structure, where one hydrogen is placed at each of the Pd-hcp and Pd-fcc sites. On the other hand, in Fig. 4 (c), both hydrogen atoms are adsorbed on the Pd-hcp sites. The structure in Fig. 4 (e) was less stable than those in Fig. 4 (c) and Fig. 4 (d), indicating that the two hydrogen atoms formed by H$_2$ cleavage prefer to be adsorbed on the Pd-hcp sites.

In the case of three hydrogen atoms, the structure in Fig. 4 (f), in which all of the hydrogen atoms are adsorbed on the Pd-hcp sites, is the most stable. When one hydrogen atom is placed on the Cu site (Fig. 4 (g)), the adsorption energy is less stable than that for Fig. 4 (f).
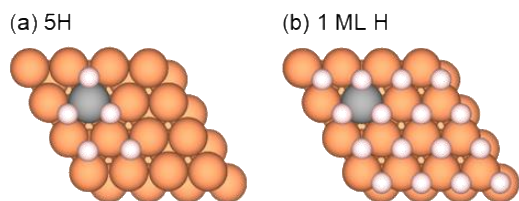
Fig. 5 Structural models of the Pd/Cu(111) surface used in DFT calculations for the core-level excitation. (a) 5 and (b) 16 H atoms were placed on the surface. Empty atoms with pseudo-atomic orbitals for hydrogen were placed on all vacant hollow sites for each structure (not shown here). The orange, gray, and small white spheres present the Cu, Pd, and H atoms, respectively.

When the number of hydrogen atoms is four, the configurations with one and three hydrogen atoms on the Cu and Pd sites (Fig. 4 (j)-(l)) are more stable than the configurations in which all of the hydrogen atoms occupy the Pd sites (Fig. 4 (h)(i)). Thus, the saturation number of hydrogen atoms at the Pd site is three.

The present calculated results show that a single Pd site can adsorb three hydrogen atoms, and the fourth and subsequent hydrogen atom would be adsorbed on the Cu site. More interestingly, the farther the distance the hydrogen atom on the Cu site from the Pd atom is, the more negative ΔH_{ad} is (see Table 1), indicating that the enthalpic stability plays an important role in hydrogen spillover. Darby et $al.$ have reported that the spillover process is driven by entropic effects.[30] The present systematic calculations clearly show that hydrogen spillover on

Table 2. The calculated binding energies (CBE) of Pd $3d_{5/2}$. The configurations in the first column correspond to those shown in Figs. 4 and 5. ΔBE in the last column is the difference of the CBE from the clean surface. The asterisk marks mean the stable structures.

Configuration	Binding energy (eV)	ΔCBE (eV)
Clean	335.7	0
1H-hcp*	335.9	0.2
2H-2NN*	336.1	0.4
2H-3NN	336.1	0.4
2H-Pd&Cu	335.9	0.2
3H-hcp*	336.2	0.5
3H-Pd&Cu	336.1	0.4
4H-all hollow	336.5	0.8
4H-hcp&top	336.8	1.1
4H-near	336.2	0.5
4H-middle	336.3	0.6
4H-far*	336.3	0.6
5H	336.4	0.7
1 ML H	336.6	0.9

Table 3. Mulliken charge populations in H, Pd, and Cu atoms.

Configuration	Mulliken charge		
	H[a]	Pd	Cu[b]
Neutral atom	1	16	19
Clean Pd/Cu(111)	-	15.86	19.12
3H-hcp	1.17	15.80	19.11
1 ML H	1.12	15.74	19.10

a Average values. b Average values of atoms surrounding the Pd atom.

the Pd/Cu SAAC surface is promoted by not only entropy, but also enthalpy.

Core-level shifts The present calculated results for the adsorption structure as a function of hydrogen coverage support the hypothesis based on the experimental results; two types of hydrogen-adsorbed Pd states exist. For the quantitative discussion for the Pd $3d_{5/2}$ binding energy observed in Fig. 3 (a), we performed the calculations for the core-level excitation.[50] The absolute binding energies of Pd $3d_{5/2}$ were calculated for the all structures in Fig. 4. In addition, we performed the calculations for the structures, where more hydrogen atoms were adsorbed as shown in Fig. 5.

The calculated binding energies (hereafter, referred to as CBE) of Pd $3d_{5/2}$ are summarized in Table 2, where the stable structures were marked with asterisks (*). On the clean surface, the CBE of Pd $3d_{5/2}$ is 335.7 eV, which shows 0.12% error compared with the experimental result (335.3 eV, the blue component in Fig. 3), which confirms the single Pd atom in Cu(111). The absolute binding energies of core levels calculated using OpenMX have a mean relative error of 0.16%,[50] and the present result was within this margin. In the case of the hydrogen adsorbed structures, the CBEs of Pd $3d_{5/2}$ systematically change to a higher binding energy as a function of the number of hydrogen atoms. The CBE for the structure in Fig. 4 (c) is 336.1 eV. The difference in the CBE between the clean and 2H-2NN configuration is 0.4 eV, consistent with the experimental results (0.4 eV between the blue and green components). Interestingly, when the number of hydrogen atoms is four or more, the CBEs of Pd $3d_{5/2}$ change to a higher energy with hydrogen atoms on the Cu site despite the same number of H-Pd. In the case of all hcp-hollow sites occupied by H atoms (Fig. 5 (b)), the CBE of Pd $3d_{5/2}$ becomes 336.7 eV. The experimental value on the hydrogen adsorbed surface is 336.4 eV (the magenta component in Fig. 3). Thus, the present calculational results support the assignments of the green and magenta component discussed in the above section. Note that the ΔCBE for the structure in Fig. 4 (i) is 1.1 eV, which seems to be consistent with the experimentally observed shift. However, this structure is very unstable (see Table 1).

The CBE of Pd$3d_{5/2}$ shifts to higher with more than four H atoms; this originates from the charge transfer from the Pd atom to H atoms through Cu atoms. The Mulliken charge populations,[63] which represent the number of valence electrons in the specific atom bonding with the other atoms, are

summarized for the four cases in Table 3. Hydrogen atoms have 1.12 electrons on average in the structure for Fig. 5 (b). Since a neutral hydrogen atom has one electron, the adsorbed H atoms stole a part of the electrons of the surface atoms. However, there was little change in the average charge of the Cu atoms surrounding the Pd atom between the clean and H-adsorbed surface (19.12 and 19.10, respectively). On the other hand, the charge of the Pd atom decreased from 15.80 to 15.74 between the 3 H and 1 ML H adsorbed surfaces (corresponding to Fig. 4 (f) and Fig. 5 (b), respectively). This behavior of the charges indicates that the decrease in electrons of Cu atoms due to hydrogen adsorption is partially compensated by the electron supply from the Pd atom. The Pd atom partly loses its electron not only due to the H adsorption at the Pd site but also due to the H adsorption on the Cu sites. Thus, the binding energy of Pd3d$_{5/2}$ shifts to higher even after the Pd site is saturated with three H atoms.

Based on the present experimental and theoretical results, we propose an atomic-scale perspective of the hydrogen
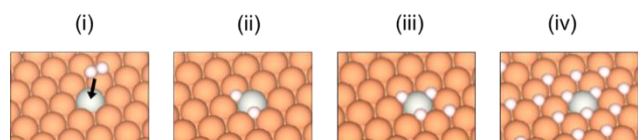
Fig. 6 The atomic-level view of the hydrogen dissociation and spillover process on the Pd/Cu SAAC surface. The orange, gray, and small white spheres represent the Cu, Pd, and H atoms, respectively. (i) a H$_2$ molecule is approaching a Pd site. (ii) Two dissociated H atoms are adsorbed on the Pd-hcp sites in the second nearest neighbor configuration. (iii) Three H atoms are adsorbed the Pd-hcp sites, and the fourth H atom is adsorbed on a Cu site. (iv) The hydrogen spillover occurs after the Pd sites are saturated by H atoms.

dissociation and spillover processes on the Pd/Cu single atom alloy catalyst surface as follows. (i) a hydrogen molecule approaches and is dissociated at the Pd site, (ii) two hydrogen atoms are adsorbed on the Pd site and occupy the hcp-hollow site in a 2NN configuration. With additional exposure, (iii) up to three hydrogen atoms are adsorbed at the Pd site. (iv) hydrogen atoms spill over onto the Cu site when Pd sites are saturated with three hydrogen atoms. We summarize these processes in Fig. 6.

Conclusions

We investigated the dissociative adsorption and spillover processes of hydrogen on the prepared Pd/Cu(111) single atom alloy catalyst surface at ~80 K using experimental and theoretical methods.

The present IRAS measurements succeeded in the direct observation of the spillover process onto the Cu sites in real-time. The H-Cu vibrational peaks were observed at 1143-1135 cm^{-1}. The development of the H-Cu peak intensity indicates that the spillover was delayed for ~260 s from the start of H$_2$ exposure. The HR-XPS results show that the Pd 3d$_{5/2}$ peaks shift to higher binding energies by hydrogen adsorption in two steps: (i) the initial occupation of the Pd site and (ii) the later spillover to the Cu sites. Systematic DFT calculations revealed the adsorption configurations during the hydrogen adsorption and

spillover processes on the Pd/Cu SAAC surface. The Pd atom can adsorb three hydrogen atoms at its hcp-hollow sites, and the fourth and subsequent hydrogen atoms spill over onto the Cu sites. We also performed the core-level calculations of Pd 3d$_{5/2}$ as a function of hydrogen coverages, which are consistent with the present experimental observations. The present experimental and theoretical results provide an atomic-scale perspective of the hydrogen dissociation and spillover processes on the Pd/Cu SAAC surface as shown in Fig. 6.

Author Contributions

W. O.: investigation, visualization, writing – original draft, and writing – review & editing; S.T.: supervision, investigation, and writing – original draft; K. M.: investigation; M. K.: software, theoretical investigation; Y. C.: investigation; F. O.: investigation; T. O.: resources, software, theoretical investigation; J.Y.: Funding acquisition, supervision, investigation, writing – original draft, and writing – review & editing.

Conflicts of interest

There are no conflicts to declare.

Acknowledgements

References

1   G. A. Olah, A. Goeppert and G. K. S. Prakash, *Beyond Oil and Gas: The Methanol Economy*, Wiley-VCH: Winheim, 2009.

2   K. Christmann, Interaction of hydrogen with solid surfaces, *Surf. Sci. Rep.*, 1988, **9**, 1–163.

3   M. S. Hofman, D. Z. Wang, Y. Yang and B. E. Koel, Interactions of incident H atoms with metal surfaces, *Surf. Sci. Rep.*, 2018, **73**, 153–189.

4   K. Fukutani, J. Yoshinobu, M. Yamauchi, T. Shima and S. Orimo, Hydrogenomics: Efficient and Selective Hydrogenation of Stable Molecules Utilizing Three Aspects of Hydrogen, *Catal. Letters*, , DOI:10.1007/s10562-021-03750-1.

5   R. I. Masel, *PRINCIPLES OF ADSORPTION AND REACTION SOLID SURFACES*, John Wiley & Sons, Inc., 1996.

6   W. Klaus, Ed., *Surface and Interface Science Volume 5: Solid-Gas Interfaces I*, WILEY-VCH, 2015, vol. 5.

7   G. C. Bond, D. A. Dowden and N. Mackenzie, The selective hydrogenation of acetylene, *Trans. Faraday Soc.*, 1958, **54**, 1537–1546.

8   J. A. Rodriguez, Physical and chemical properties of bimetallic surfaces, *Surf. Sci. Rep.*, 1996, **24**, 223–287.

9   J. G. Chen, C. A. Menning and M. B. Zellner, Monolayer bimetallic surfaces: Experimental and theoretical studies of trends in electronic and chemical properties, *Surf. Sci. Rep.*, 2008, **63**, 201–254.

10   R. T. Hannagan, G. Giannakakis, M. Flytzani-Stephanopoulos and E. C. H. Sykes, Single-Atom Alloy Catalysis, *Chem. Rev.*, 2020, **120**, 12044–12088.

11   G. Giannakakis, M. Flytzani-Stephanopoulos and E. C. H. Sykes, Single-Atom Alloys as a Reductionist Approach to the Rational Design of Heterogeneous Catalysts, *Acc. Chem. Res.*, 2019, **52**, 237–247.

12   J. P. Simonovis, A. Hunt and I. Waluyo, In situ ambient pressure XPS study of Pt/Cu(111) single-atom alloy in catalytically relevant reaction conditions, *J. Phys. D. Appl. Phys.*, , DOI:10.1088/1361-6463/abe07f.

13   M. K. Abdel-Rahman and M. Trenary, Propyne Hydrogenation over a Pd/Cu(111) Single-Atom Alloy Studied using Ambient Pressure Infrared Spectroscopy, *ACS Catal.*, 2020, **10**, 9716–9724.

14   G. Kyriakou, M. B. Boucher, A. D. Jewell, E. A. Lewis, T. J. Lawton, A. E. Baber, H. L. Tierney, M. Flytzani-stephanopoulos and E. C. H. Sykes, Isolated Metal Atom Geometries as a Strategy for Selective Heterogeneous Hydrogenations, *Science*, 2012, **335**, 1209–1213.

15   M. D. Marcinkowski, A. D. Jewell, M. Stamatakis, M. B. Boucher, E. A. Lewis, C. J. Murphy, G. Kyriakou and E. C. H. Sykes, Controlling a spillover pathway with the molecular cork effect, *Nat. Mater.*, 2013, **12**, 523–528.

16   F. Qin and W. Chen, Copper-based single-atom alloys for heterogeneous catalysis, *Chem. Commun.*, 2021, **57**, 2710–2723.

17   J. Shan, J. Liu, M. Li, S. Lustig, S. Lee and M. Flytzani-Stephanopoulos, NiCu single atom alloys catalyze the C–H bond activation in the selective non- oxidative ethanol dehydrogenation reaction, *Appl. Catal. B Environ.*, 2018, **226**, 534–543.

18   M. B. Boucher, M. D. Marcinkowski, M. L. Liriano, C. J. Murphy, E. A. Lewis, A. D. Jewell, M. F. G. Mattera, G. Kyriakou, M. Flytzani-Stephanopoulos and E. C. H. Sykes, Molecular-scale perspective of water-catalyzed methanol dehydrogenation to formaldehyde, *ACS Nano*, 2013, **7**, 6181–6187.

19   C. M. Kruppe, J. D. Krooswyk and M. Trenary, Selective Hydrogenation of Acetylene to Ethylene in the Presence of a Carbonaceous Surface Layer on a Pd/Cu(111) Single-Atom Alloy, *ACS Catal.*, 2017, **7**, 8042–8049.

20   M. B. Boucher, B. Zugic, G. Cladaras, J. Kammert, M. D. Marcinkowski, T. J. Lawton, E. C. H. Sykes and M. Flytzani-Stephanopoulos, Single atom alloy surface analogs in $Pd_{0.18}Cu_{15}$ nanoparticles for selective hydrogenation reactions, *Phys. Chem. Chem. Phys.*, 2013, **15**, 12187–12196.

21   R. Réocreux, M. Uhlman, T. Thuening, P. Kress, R. Hannagan, M. Stamatakis and E. C. H. Sykes, Efficient and selective carbon-carbon coupling on coke-resistant PdAu single-atom alloys, *Chem. Commun.*, 2019, **55**, 15085–15088.

22   M. D. Marcinkowski, J. Liu, C. J. Murphy, M. L. Liriano, N. A. Wasio, F. R. Lucci, M. Flytzani-Stephanopoulos and E. C. H. Sykes, Selective Formic Acid Dehydrogenation on Pt-Cu Single-Atom Alloys, *ACS Catal.*, 2017, **7**, 413–420.

23   M. T. Darby, F. R. Lucci, M. D. Marcinkowski, A. J. Therrien, A. Michaelides, M. Stamatakis and E. C. H. Sykes, Carbon Monoxide Mediated Hydrogen Release from PtCu Single-Atom Alloys: The Punctured Molecular Cork Effect, *J. Phys. Chem. C*, 2019, **123**, 10419–10428.

24   M. D. Marcinkowski, M. T. Darby, J. Liu, J. M. Wimble, F. R. Lucci, S. Lee, A. Michaelides, M. Flytzani-Stephanopoulos, M. Stamatakis and E. C. H. Sykes, Pt/Cu single-atom alloys as coke-resistant catalysts for efficient C-H activation, *Nat. Chem.*, 2018, **10**, 325–332.

25   H. L. Tierney, A. E. Baber, J. R. Kitchin and E. C. H. Sykes, Hydrogen dissociation and spillover on individual isolated palladium atoms, *Phys. Rev. Lett.*, 2009, **103**, 1–4.

26   M. Ramos, A. E. Martínez and H. F. Busnengo, H_2 dissociation on individual Pd atoms deposited on Cu(111), *Phys. Chem. Chem. Phys.*, 2012, **14**, 303–310.

27   Q. Fu and Y. Luo, Catalytic activity of single transition-metal atom doped in Cu(111) surface for heterogeneous hydrogenation, *J. Phys. Chem. C*, 2013, **117**, 14618–14624.

28   A. E. Baber, H. L. Tierney, T. J. Lawton and E. C. H. Sykes, An atomic-scale view of palladium alloys and their ability to dissociate molecular hydrogen, *ChemCatChem*, 2011, **3**, 607–614.

29   G. Kyriakou, E. R. M. Davidson, G. Peng, L. T. Roling, S. Singh, M. B. Boucher, M. D. Marcinkowski, M. Mavrikakis, A. Michaelides and E. C. H. Sykes, Significant quantum effects in hydrogen activation, *ACS Nano*, 2014, **8**, 4827–4835.

30   M. T. Darby, R. Réocreux, E. C. H. Sykes, A. Michaelides and M. Stamatakis, Elucidating the Stability and Reactivity of Surface Intermediates on Single-Atom Alloy Catalysts, *ACS Catal.*, 2018, **8**, 5038–5050.

31   Q. Fu and Y. Luo, Active sites of Pd-doped flat and stepped Cu(111) surfaces for H_2 dissociation in heterogeneous catalytic hydrogenation, *ACS Catal.*, 2013, **3**, 1245–1252.

32   K. Mudiyanselage, Y. Yang, F. M. Hoffmann, O. J. Furlong, J. Hrbek, M. G. White, P. Liu and D. J. Stacchiola, Adsorption of hydrogen on the surface and sub-surface of Cu(111), *J. Chem. Phys.*, , DOI:10.1063/1.4816515.

33   G. Lee, D. B. Poker, D. M. Zehner and E. W. Plummer, Coverage and structure of deuterium on Cu(111), *Surf. Sci.*, 1996, **357–358**, 717–720.

34   W. Kirstein, B. Krüger and F. Thieme, CO adsorption studies on pure and Ni-covered Cu(111) surfaces, *Surf. Sci.*, 1986, **176**, 505–529.

35   R. Raval, S. F. Parker, M. E. Pemble, P. Hollins, J. Pritchard and M. A. Chesters, FT-RAIRS, EELS and LEED studies of the

adsorption of carbon monoxide on Cu(111), *Surf. Sci.*, 1988, **203**, 353–377.

36 H. L. Tierney, A. E. Baber and E. C. H. Sykes, Atomic-scale imaging and electronic structure determination of catalytic sites on Pd/Cu near surface alloys, *J. Phys. Chem. C*, 2009, **113**, 7246–7250.

37 J. J. Yeh and I. Lindau, Atomic subshell photoionization cross sections and aymmetry parameters: 1⩽Z⩽103, *At. Data Nucl. Data Tables*, 1985, **32**, 1–155.

38 I. M. Band, Y. I. Kharitonov and M. B. Trzhaskovskaya, Photoionization cross sections and photoelectron angular distributions for x-ray line energies in the range 0.132-4.509 keV Targets: 1 ⩽ Z ⩽ 100, *At. Data Nucl. Data Tables*, 1979, **23**, 443–505.

39 W. Klaus, Ed., *Surface and Interface Science Volume 1: Concepts and Methods*, Wiley-VCH, 2012.

40 The code, OpenMX, pseudoatomic basis functions, and pseudopotentials are available at http://www.openmx-square.org.

41 T. Ozaki and H. Kino, Efficient projector expansion for the ab initio LCAO method, *Phys. Rev. B - Condens. Matter Mater. Phys.*, 2005, **72**, 1–8.

42 J. P. Perdew, K. Burke and M. Ernzerhof, Generalized gradient approximation made simple, *Phys. Rev. Lett.*, 1996, **77**, 3865–3868.

43 K. Lejaeghere, G. Bihlmayer, T. Björkman, P. Blaha, S. Blügel, V. Blum, D. Caliste, I. E. Castelli, S. J. Clark, A. Dal Corso, S. De Gironcoli, T. Deutsch, J. K. Dewhurst, I. Di Marco, C. Draxl, M. Dułak, O. Eriksson, J. A. Flores-Livas, K. F. Garrity, L. Genovese, P. Giannozzi, M. Giantomassi, S. Goedecker, X. Gonze, O. Grånäs, E. K. U. Gross, A. Gulans, F. Gygi, D. R. Hamann, P. J. Hasnip, N. A. W. Holzwarth, D. Iuşan, D. B. Jochym, F. Jollet, D. Jones, G. Kresse, K. Koepernik, E. Küçükbenli, Y. O. Kvashnin, I. L. M. Locht, S. Lubeck, M. Marsman, N. Marzari, U. Nitzsche, L. Nordström, T. Ozaki, L. Paulatto, C. J. Pickard, W. Poelmans, M. I. J. Probert, K. Refson, M. Richter, G. M. Rignanese, S. Saha, M. Scheffler, M. Schlipf, K. Schwarz, S. Sharma, F. Tavazza, P. Thunström, A. Tkatchenko, M. Torrent, D. Vanderbilt, M. J. Van Setten, V. Van Speybroeck, J. M. Wills, J. R. Yates, G. X. Zhang and S. Cottenier, Reproducibility in density functional theory calculations of solids, *Science*, DOI:10.1126/science.aad3000.

44 T. Ozaki, Variationally optimized atomic orbitals for large-scale electronic structures, *Phys. Rev. B*, 2003, **67**, 155108.

45 I. Morrison, D. M. Bylander and L. Kleinman, Nonlocal Hermitian norm-conserving Vanderbilt pseudopotential, *Phys. Rev. B*, 1993, **47**, 6728.

46 G. Theerich and N. A. Hill, Self-consistent treatment of spin-orbit coupling in solids using relativistic fully separable ab initio pseudopotentials, *Phys. Rev. B*, 2001, **64**, 073106.

47 Database (2019) of optimized VPS and PAO, https://t-ozaki.issp.u-tokyo.ac.jp/vps_pao2019/.

48 S. Grimme, S. Ehrlich and L. Goerigk, Effect of the damping function in dispersion corrected density functional theory, *J. Comput. Chem.*, 2011, **32**, 1456–1465.

49 S. Grimme, J. Antony, S. Ehrlich and H. Krieg, A consistent and accurate ab initio parametrization of density functional dispersion correction (DFT-D) for the 94 elements H-Pu, *J. Chem. Phys.*, 2010, **132**, 154104.

50 T. Ozaki and C. C. Lee, Absolute Binding Energies of Core Levels in Solids from First Principles, *Phys. Rev. Lett.*, 2017, **118**, 1–5.

51 Database (2019) of optimized VPS and PAO for core level excitations, https://t-ozaki.issp.u-tokyo.ac.jp/vps_pao_core2019/.

52 E. M. Mccash, S. F. Parker, J. Pritchard and M. A. Chesters, The adsorption of atomic hydrogen on Cu(111) investigated by reflection-absorption infrared spectroscopy, electron energy loss spectroscopy and low energy electron diffraction, *Surf. Sci.*, 1989, **215**, 363–377.

53 C. M. Kruppe, J. D. Krooswyk and M. Trenary, Polarization-Dependent Infrared Spectroscopy of Adsorbed Carbon Monoxide to Probe the Surface of a Pd/Cu(111) Single-Atom Alloy, *J. Phys. Chem. C*, 2017, **121**, 9361–9369.

54 P. Hollins, The influence of surface defects on the infrared spectra of adsorbed species, *Surf. Sci. Rep.*, 1992, **16**, 51–94.

55 J. H. Hubbell and S. M. Seltzer, The software of "NIST ELECTRON EFFECTIVE-ATTENUATION-LENGTH DATABASE version 1.3" can be dowonloaded at https://www.nist.gov/srd/nist-standard-reference-database-82.

56 M. J. Gladys, A. A. El Zein, A. Mikkelsen, J. N. Andersen and G. Held, Chemical composition and reactivity of water on clean and oxygen-covered Pd{1 1 1}, *Surf. Sci.*, 2008, **602**, 3540–3549.

57 S. Surnev, M. Sock, M. G. Ramsey, P. P. Netzer, M. Wiklund, M. Borg and J. N. Andersen, CO adsorption on Pd(111): A high-resolution core level photoemission and electron energy loss spectroscopy study, *Surf. Sci.*, 2000, **470**, 171–185.

58 J. Tang, S. Yamamoto, T. Koitaya, A. Yoshigoe, T. Tokunaga, K. Mukai, I. Matsuda and J. Yoshinobu, Mass transport in the PdCu phase structures during hydrogen adsorption and absorption studied by XPS under hydrogen atmosphere, *Appl. Surf. Sci.*, 2019, **480**, 419–426.

59 J. Tang, O. Seo, D. S. R. Rocabado, T. Koitaya, S. Yamamoto, Y. Nanba, C. Song, J. Kim, A. Yoshigoe, M. Koyama, S. Dekura, H. Kobayashi, H. Kitagawa, O. Sakata, I. Matsuda and J. Yoshinobu, Hydrogen absorption and diffusion behaviors in cube-shaped palladium nanoparticles revealed by ambient-pressure X-ray photoelectron spectroscopy, *Appl. Surf. Sci.*, 2022, **587**, 152797.

60 B. J. Hinch and L. H. Dubois, Stable and metastable phases of water adsorbed on Cu(111), *J. Chem. Phys.*, 1992, **96**, 3262–3266.

61 M. T. Darby, E. C. H. Sykes, A. Michaelides and M. Stamatakis, Carbon Monoxide Poisoning Resistance and Structural Stability of Single Atom Alloys, *Top. Catal.*, 2018, **61**, 428–438.

62 A. Bach Aaen, E. Laegsgaard, A. V. Ruban and I. Stensgaard, Submonolayer growth of Pd on Cu(111) studied by

scanning tunneling microscopy, *Surf. Sci.*, 1998, **408**, 43–56.

63   R. S. Mulliken, Electronic Population Analysis on LCAO, *J. Chem. Phys*, 1955, **23**, 1833.